Seizures, spreading depolarizations and sudden death

Jansen, N.A.

Chapter 6

Brainstem depolarization –induced lethal apnea associated with gain-of-function *SCN1A*^{L263V} is prevented by sodium channel blockade

Nico A. Jansen
Sandrine Cestèle
Silvia Sanchez Marco
Maarten Schenke
Kirsty Stewart
Jayesh Patel
Else A. Tolner
Andreas Brunklaus
Massimo Mantegazza
Arn M.J.M. van den Maagdenberg

Proc Natl Acad Sci U S A 2024;121(14):e2309000121

ABSTRACT

Apneic events are frightening but largely benign events that often occur in infants. Here we report apparent life-threatening apneic events in an infant with the homozygous *SCN1A*^{L263V} missense mutation, which causes familial hemiplegic migraine type 3 (FHM3) in heterozygous family members, in the absence of epilepsy. Observations consistent with the events in the infant were made in an *Scn1a*^{L263V} knock-in mouse model, in which apnea was preceded by a large brainstem DC-shift, indicative of profound brainstem depolarization. The L263V mutation caused gain of $Na_V1.1$ function effects in transfected HEK293 cells. Sodium channel blockade mitigated the gain-of-function characteristics, rescued lethal apnea in *Scn1a*^{L263V} mice, and decreased the frequency of severe apneic events in the patient. Hence, this study shows that *SCN1A*^{L263V} can cause life-threatening apneic events, which in a mouse model were caused by profound brainstem depolarization. In addition to being potentially relevant to sudden infant death syndrome (SIDS) pathophysiology, these data indicate that sodium channel blockers may be considered as therapeutic for apneic events in patients with these and other gain-of-function *SCN1A* mutations.

INTRODUCTION

Breath-holding spells are apneic events that are common in infants, often occur following emotional provocation, and can lead to loss of consciousness in severe cases.[1] Despite the often frightening appearance these events are considered benign. Prolonged apnea requiring resuscitation is rare, and other abnormalities have been suggested to contribute to apnea in these cases.[1] It is unclear to what extent there is a correlation between these apneic events and sudden infant death syndrome (SIDS).[2, 3] Although genetic factors that predispose to breath-holding spells largely remain to be identified, genetic variants have been associated with SIDS and other sudden death phenotypes together referred to as sudden unexpected death in pediatrics (SUDP), including sudden unexplained death in childhood (SUDC) and sudden unexpected death in epilepsy (SUDEP). Of these, variants in genes encoding voltage-gated sodium channels seem relatively abundant,[4] including variants in *SCN1A*.[4-8]

Here, we report a clinical case of unusually severe apneic events that resulted in apparent life-threatening events. Family history and genetic analyses revealed the presence of hemiplegic migraine caused by a heterozygous *SCN1A*^{L263V} missense mutation in family members, consistent with a diagnosis of familial hemiplegic migraine type 3 (FHM3), and homozygosity of the mutation in the reported case. The *SCN1A* gene encodes the α1 subunit of voltage-gated $Na_V1.1$ sodium channels and FHM3 mutations cause a gain of sodium channel function observed in heterologous expression systems[9, 10] and in an *Scn1a*^{L1649Q} knock-in FHM3 mouse model.[11] Apneic events are not typically associated with FHM, except for anecdotal reports of unexplained respiratory arrest[12] or apnea following general anesthesia[13] but these studies did not investigate the genetic cause underlying these phenotypes. Notably, typical FHM3 phenotypes are milder and mostly involve pure hemiplegic migraine attacks.[14, 15]

In this study, we investigated *Scn1a*^{L263V} knock-in mice, modelling the mutation found in the clinical case. *Scn1a*^{L263V} mice died prematurely due to spontaneous sudden apnea preceded by a large brainstem DC-shift, indicative of profound brainstem depolarization, involving the ventrolateral medulla, a brainstem region vital for generating breathing rhythm,[16, 17] in the absence of epileptiform activity. The mutation resulted in gain-of-function effects on sodium currents in transfected HEK293 cells, which could be mitigated by sodium channel blockers. Similarly, sodium channel blockade prevented apnea in *Scn1a*^{L263V} mice and reduced the frequency of severe apneic events in the clinical case. Thus, *SCN1A*^{L263V} can cause life-threatening apneic events and sodium channel blockers may be considered as therapeutic for patients with these or other gain-of-function *SCN1A* mutations at risk of sudden death.

RESULTS

Severe apneic events in a homozygous *SCN1A*^{L263V} patient in a familial hemiplegic migraine type 3 family

The clinical case (proband; III-1; Fig. 1B) experienced at 2 months of age an apparent life-threatening event. She became distressed and started crying while lying in her cradle during which she became unresponsive, hypotonic, apneic and pale with progressive cyanosis for 5 minutes, requiring physical stimulation to recover. Another apparent life-threatening event occurred at 9 months of age that appeared initiated by agitation. Workup in the hospital at the time did not reveal cardiac abnormalities, and the mother (II-4) was instructed on how to use a manual resuscitator. Between 9-17 months of age, the child experienced approximately 40 apneic events (interpreted as breath-holding spells by the clinicians) that appeared provoked by agitation (crying), during which she became stiff for 2-3 s, then floppy and unresponsive. The mother performed manual resuscitation during the majority of events, and the child regained consciousness within 30-60 s. Obstetric history included maternal gestational diabetes with unremarkable delivery. The child showed normal development until the age of 17 months, although mild speech delay was noticed. At 17 months of age she presented to the emergency department. Previously at home, she became agitated and suddenly stopped breathing after which she lost responsiveness. Cardiopulmonary resuscitation was initiated by the mother and continued by paramedics 6 minutes after the incident; 15 minutes after the incident cardiac output resumed. At the ICU, neuroprotective measures including morphine and midazolam sedation were initiated. During the pediatric ICU stay, hypotension developed that required inotropic support, remaining further uncomplicated. After 72 hours, the child was extubated. MRI showed findings consistent with hypoxic-ischemic brain injury in the basal ganglia (Fig. 1C). There were no abnormalities in other brain regions, including the hippocampi or brainstem. EEG showed high-voltage irregular activity with no epileptiform features. During admission, the patient underwent long-term video EEG recording. The resting record showed no epileptiform abnormality or evidence of subclinical seizures. Two typical events were recorded, one of which requiring resuscitation. The electrographic correlates were widespread rhythmic slow waves of increasing amplitude leading to a period of attenuation and quick return to baseline activity. There was relative bradycardia during the episodes. The sequence of EEG changes was consistent with a physiological response to cerebral hypoxia and the events were in keeping with breath-holding spells without epileptiform features. Similarly, previous wake and sleep EEG recordings at age 2 months following an acute life-threatening episode, and at 7 months showed no epileptiform discharges. ECG and echocardiograms during admissions were normal, however, they did not capture any apneic events. The loop recorder showed sinus rhythm and sinus bradycardia with some possible junctional rhythm (probably during apneic events) with some frequent atrial ectopics.

Family history was negative for breath-holding spells. A sibling (III-2) passed away at 2 years of age from an undetermined cause. She had a history of febrile tonic-clonic seizures associated

with an infectious illness on each occasion. Autopsy revealed severe laryngotracheobronchitis. Several family members were diagnosed with hemiplegic migraine (Fig. 1A and B). The mother of the proband (II-4) was diagnosed with hemiplegic migraine, following several dozen attacks of migraine with auras that included unilateral motor weakness, confusion, and word finding difficulties. The mother's half-sister (II-1), half-brother (II-2) and father (I-2) also had hemiplegic migraine, presenting with similar symptoms. The proband's half-sister (III-3) has presented similar symptoms and she is pending clinical assessment. None of the family members affected by hemiplegic migraine had a history of seizures. Genetic analyses on DNA samples from the proband's maternal side of the family revealed a heterozygous missense mutation in exon 6 of the *SCN1A* gene replacing a leucine for a valine residue at position 263 of the $Na_V1.1$ α1 subunit (Fig. 1A). The mutation co-segregated with all family members with hemiplegic migraine. The heterozygous *SCN1A*^{L263V} mutation was also found in the proband's half-sister (III-3). Most notably, a homozygous *SCN1A*^{L263V} mutation was found in the proband. True homozygosity of the *SCN1A*^{L263V} allele was confirmed by intragenic markers rs994399 (T-allele), rs1542484 (C-allele), rs7580482 (G-allele), rs6432860 (C-allele) and rs2298771 (A-allele) and dosage analysis by multiplex ligation-dependent probe amplification across the *SCN1A* gene. The proband had a gene panel of 1117 epilepsy and arrhythmia genes performed (including *SCN2A*, *SCN3A*, *SCN5A*, *SCN8A* and *MECP2*), which was negative apart from *SCN1A*.

Treatment with levetiracetam (40 mg/kg/day) was initiated in the proband during the pediatric ICU stay, which appeared to have no effect on apneic events (Fig. 1D). Considering the presence of an *SCN1A*^{L263V} mutation, which previously was shown to exert gain-of-function effects in transfected HEK293 cells,[9] treatment with the sodium channel blocker carbamazepine (CBZ; 10 mg/kg/day) was initiated. This was followed by a marked decrease in severity of apneic events (Fig. 1D).

FIGURE 1A-1B. A patient with homozygosity for the *SCN1A*^{L263V} mutation in a familial hemiplegic migraine type 3 family.

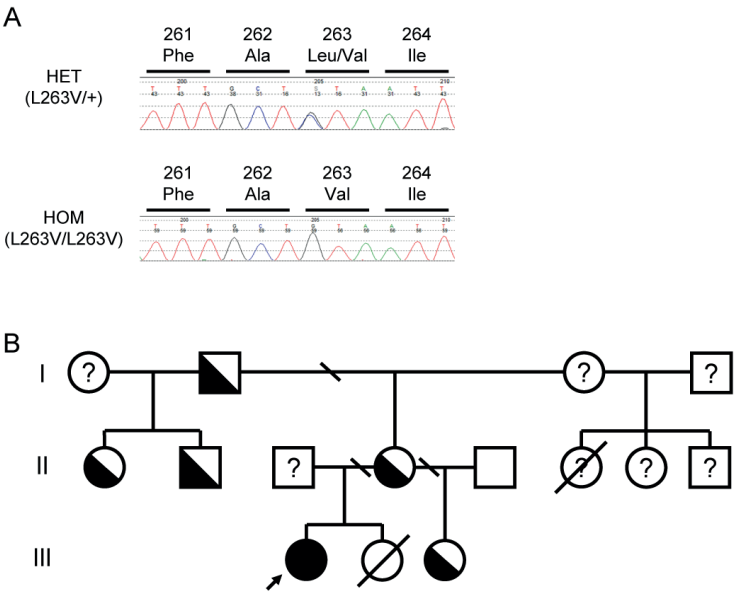

(A) Electropherograms showing single or double copy of the C→G nucleotide change in codon 263 of exon 6 of the *SCN1A* gene, respectively in heterozygous and homozygous carriers. **(B)** Pedigree of the patient's family, showing heterozygous (half-filled) and homozygous (proband (indicated by the arrow); filled) carriers of the *SCN1A*^{L263V} mutation, as well as wild-type (empty) and non-tested (question mark) family members.

FIGURE 1C-1D. A patient with homozygosity for the *SCN1A*^{L263V} mutation in a familial hemiplegic migraine type 3 family.

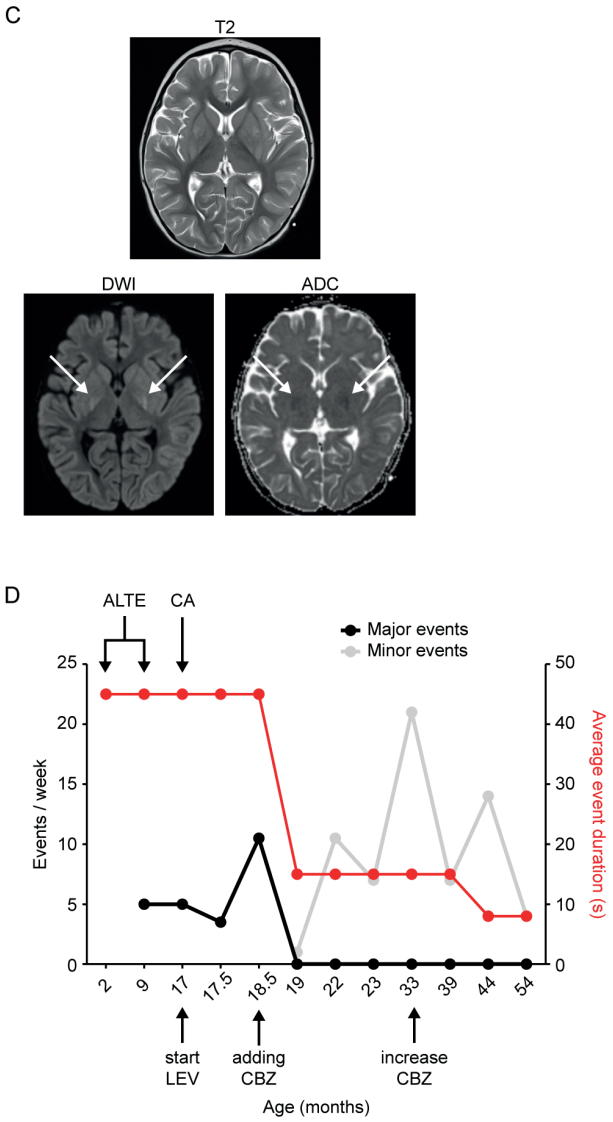

(C) Axial brain 3T MR images obtained from the proband at 17 months following an episode of severe apnea and cardiac arrest requiring cardiopulmonary resuscitation, showing T2-weighted hyperintensity of the basal ganglia bilaterally (top) with areas of restricted diffusion (bottom, arrows), consistent with hypoxic-ischemic brain injury. **(D)** Frequency (black and grey) and duration (red) of apneic events in the proband, with particularly severe events indicated by arrows at the top (ALTE=apparent life-threatening event; CA=cardiac arrest). Note that event duration was not affected by levetiracetam (LEV; 40 mg/kg/day), but decreased following addition of carbamazepine (CBZ; 10 mg/kg/day). Although an increase in minor events (lasting 5-10 s) was observed (grey line), this may reflect an increased awareness of the caregiver and/or physician for such events, which was nevertheless followed by an increase in CBZ dosage to 17 mg/kg/day at 33 months.

Sudden death in *Scn1a*^{L263V} mice is preceded by apnea and a brainstem DC-shift

To investigate the potential mechanism of apneic events in the proband, we studied heterozygous and homozygous mice with the same L263V missense mutation, introduced in the orthologous *Scn1a* gene using a CRISPR/Cas9 strategy.[18] Heterozygous *Scn1a*^{L263V} mice show decreased survival with peak mortality in postnatal weeks 3-4, without overt behavioral abnormalities other than sudden short-lasting behavior in the seconds preceding fatality.[18] We implanted 23 heterozygous *Scn1a*^{L263V} mice to record brain and (cardio)respiratory activity starting from postnatal day 20-21. During 2-week video-EEG recordings, 22 mice died after 104±21 (range 14-332) hours. None of the animals showed cortical epileptiform activity (example in Movie S1). Recordings of cortical and hippocampal activity in a separate group of 8 *Scn1a*^{L263V} mice (total 926 (range 12-264) hours recording time) showed no seizures, spike-and-wave discharges or interictal spikes (examples in SI Appendix, Fig. S1). In the mice that survived > 24 hours after surgery (n=19/22 mice), fatal events more often occurred during the dark phase (6:30 PM-6:30 AM; 15/19 mice, P=0.001, Fisher's test). All mice were awake before the fatal event commenced, as evidenced by video recordings and vigilance state assessment from EEG data. In the majority of mice (n=16/22) behavior lasted only 1-2 s comprising sudden change of posture with (subtle) hindlimb extension (example in Movie S2). In the remaining 6 mice, this was preceded by wild running lasting 7±1.4 (range 2-12) s. Early mortality in homozygous *Scn1a*^{L263V} mice (n=8; postnatal age 16.9±0.3 (range 15-18) days) precluded EEG recordings, due to insufficient recovery from surgery to allow for chronic invasive recordings. However, video recordings from homozygous *Scn1a*^{L263V} mice (n=6) that did not undergo surgery showed behaviors including hindlimb extension (n=6) and wild running (n=3) during fatal events which lasted 1-12 s, similar to what was observed in heterozygous operated mice. When compared to wild-type (WT) mice, heterozygous or homozygous *Scn1a*^{L263V} mice did not show abnormalities in baseline behavior or body weight (6.2±0.3, 5.9±0.3 and 6.5±0.2 g at P14, respectively; n=6 per group; P=0.26, ANOVA).

In 6 heterozygous *Scn1a*^{L263V} mice, recordings of respiratory activity, ECG and EEG revealed a stereotypical pattern involving sudden apnea coinciding with transient bradycardia, followed by EEG suppression (example in Fig. 2). In an FHM1 mouse model, seizure-related apnea was caused by brainstem medullary spreading depolarization.[19] To study whether a similar mechanism may occur here, we implanted heterozygous *Scn1a*^{L263V} mice (n=17) with an electrode in the ventrolateral medulla. In all animals that died during the 2-week recording period (n=16, of which 13 with respiratory and 6 with ECG recordings), a DC-shift occurred during abnormal behavior associated with the fatal event (example in Movie S3) that was immediately followed by apnea and (transient) bradycardia (Fig. 3A and B), preceding EEG suppression, cortical anoxic depolarization (AD) and cardiac arrest (Fig. 3C). Respiratory and ECG recordings showed no abnormalities preceding this event. These findings indicate that *Scn1a*^{L263V} mice show brainstem depolarization-associated apnea resulting in sudden death.

FIGURE 2. Example of brain and cardiorespiratory recordings during spontaneous sudden death in a heterozygous *Scn1a*^{L263V} mouse.

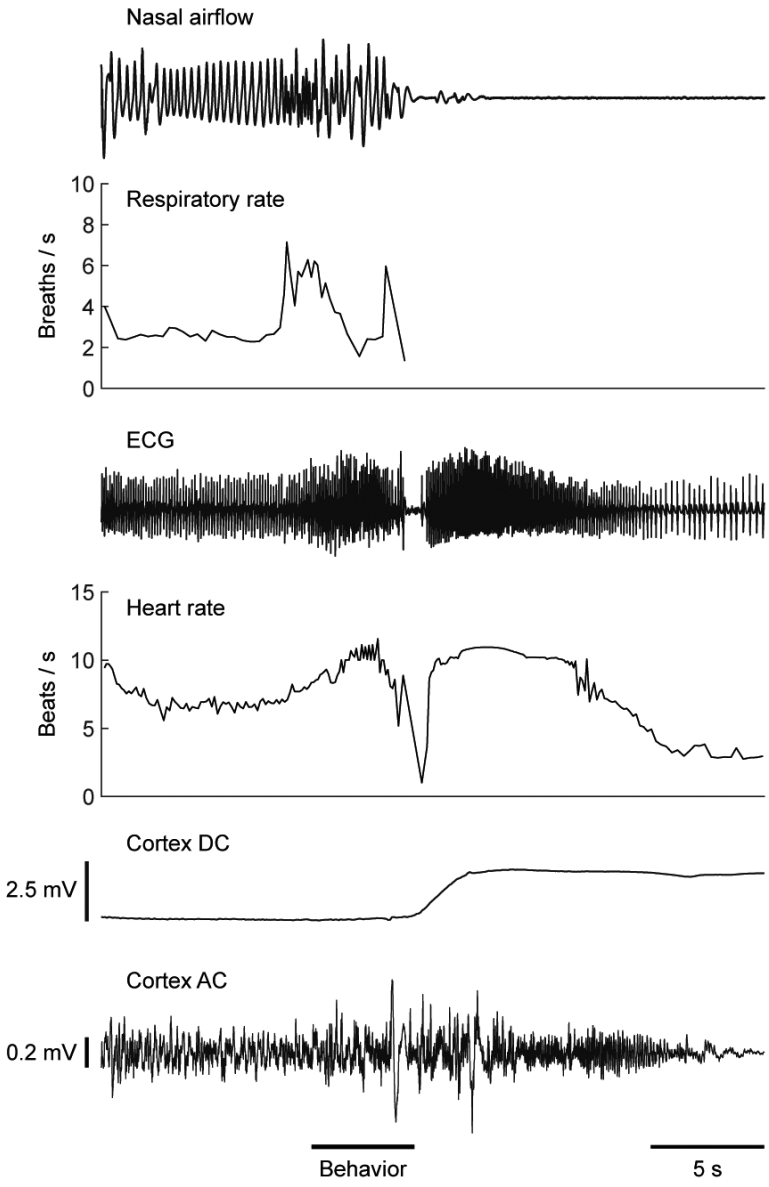

Note that the sudden onset of apnea coincided with transient bradycardia, and preceded suppression of electrocorticogram activity (cortex AC).

FIGURE 3A. Lethal sudden apnea in heterozygous *Scn1a*^{L263V} mice is preceded by a DC-shift in the medulla.

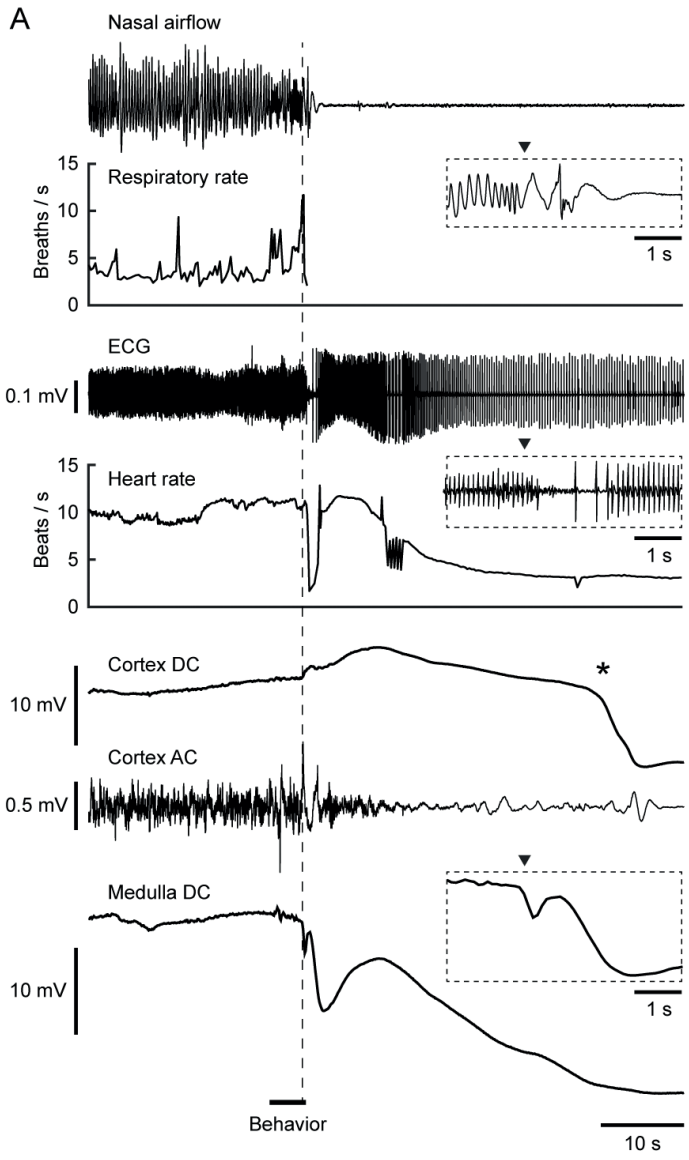

(A) Spontaneous sudden apnea and bradycardia follow soon after onset of a DC-shift in the ventrolateral medulla (dashed line, corresponding to arrowheads in insets) in an *Scn1a*^{L263V} mouse.

FIGURE 3B-3C. Lethal sudden apnea in heterozygous *Scn1a*^{L263V} mice is preceded by a DC-shift in the medulla.

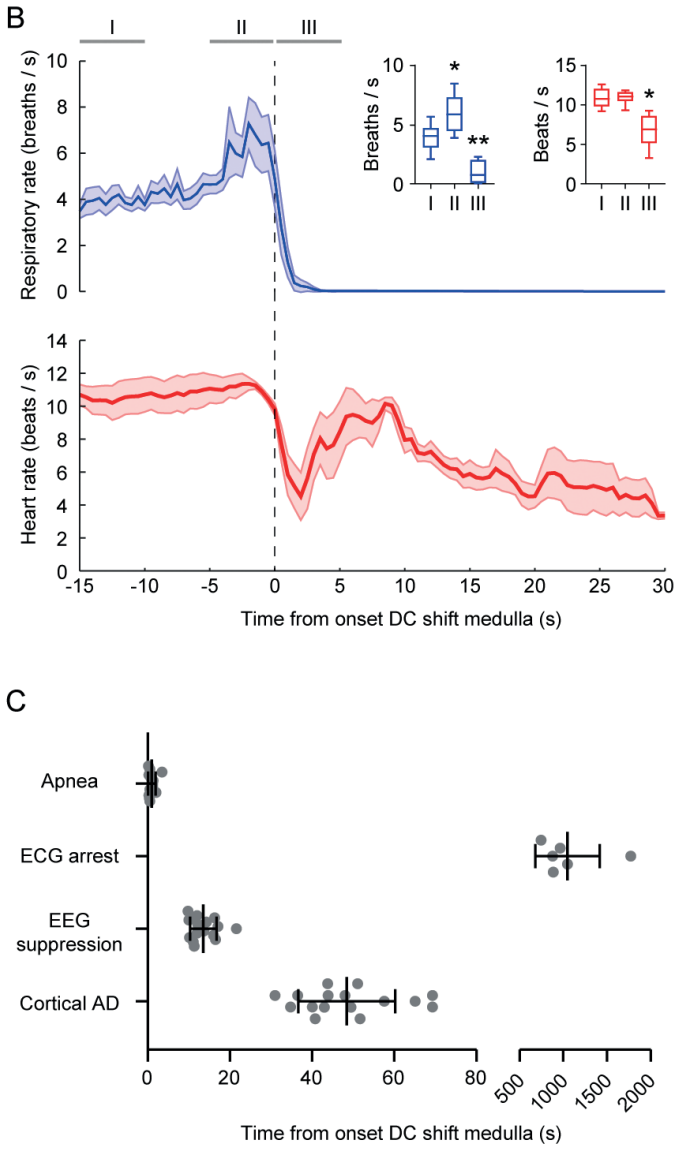

(B) Similar dynamics were observed in recordings from all *Scn1a*^{L263V} mice (n=13 with respiratory recordings, n=6 with ECG), here aligned at onset of the medullary DC-shift (dashed line). When compared to baseline (I), respiratory rate was significantly increased prior to the DC-shift (II), while both respiratory and heart rate were decreased immediately after the DC-shift (III; *P<0.05, **P<0.005, repeated measures ANOVA with Dunnett's test). **(C)** Timing of arrest of brain and cardiorespiratory activity with respect to the medullary DC-shift. A consistent sequence of apnea, EEG suppression, cortical anoxic depolarization (AD) and cardiac arrest was observed in all animals.

A profound brainstem depolarization precedes local and cortical hypoxia in *Scn1a*^{L263V} mice

The brainstem DC-shift suggests that a profound depolarization underlies apnea in *Scn1a*^{L263V} mice. Depolarizations such as those occurring in spreading depolarization (SD) are known to propagate through contiguous grey matter with a speed of several millimeters per minute, and this speed appears lower in brainstem regions.[20] The sudden nature of the events observed in *Scn1a*^{L263V} mice indicates that depolarizations occur either in a limited region crucial for cardiorespiratory functioning, are multifocal and/or propagate at atypically high velocities. To investigate this, we implanted *Scn1a*^{L263V} mice with (bipolar) electrodes in the pons (n=5), and/or contralateral medulla (n=6), in addition to the ventrolateral medulla. Of note, DC-shifts initiated within 2 s from one another and were associated with a transient increase in local multi-unit activity (MUA; Fig. 4A and 5A), which closely paralleled respiratory failure (Fig. 5B). Delay between DC-shifts was greater for ipsi- versus contralateral medulla than for (ipsilateral) pons versus medulla (1.05±0.26 and 0.18±0.08 s, respectively; $t_{(5.9)}$=3.14, P=0.02, Welch's t-test). This yielded estimated propagation velocities of 1.5-14.4 (median 1.9) mm/s and 2.2-20.2 (median 7.8) mm/s between electrodes in medulla-medulla and pons-medulla, respectively. Brainstem DC-shifts had a characteristic shape consisting of an initial steep depolarizing phase with an amplitude of 6.7±0.7 (range 4.9-15.5) mV, followed by plateauing and finally a more persistent potential drop.

Hypoxia can induce SD at multiple foci, [21] which, in the absence of detailed spatial information, complicates the interpretation of DC-shift propagation patterns. Although the sudden onset of apnea during/after the DC-shift suggests that global hypoxia does not precede the DC-shift, local hypoxia may be present. Therefore, we performed simultaneous tissue partial oxygen pressure (PO_2) recordings in the medulla and cortex (n=4) while freely behaving *Scn1a*^{L263V} mice were electrically stimulated in the inferior colliculus (20-100 μA, 50 Hz, 1-ms bipolar pulses for 2 s) – a paradigm that induced brainstem SD in an FHM1 mouse model.[19] Here, all 4 *Scn1a*^{L263V} mice showed fatal apnea 29±9 (range 1-52) s after stimulating with the minimal current intensity eliciting behavior which commenced with a startle response (38±13 μA), which was in all animals followed by running (lasting 1-14 s), immobility and hindlimb extension. Similar to spontaneous events, apnea was preceded by DC-shifts in the brainstem (Fig. 4B). In WT littermates (n=5), stimulation of the inferior colliculus induced a similar startle response followed by running behavior (lasting 1-8 s), but no hindlimb extension, apnea or death, despite increasing current intensities to twice the minimum required to elicit behavior. Tissue PO_2 recordings in *Scn1a*^{L263V} mice indicated normoxia at apnea onset in the medulla and cortex (39.1±5.1 and 29.1±2 mmHg, respectively), but PO_2 dropped to hypoxic levels (<10 mmHg) soon after onset of apnea, which invariably occurred earlier in medulla compared to cortex (Fig. 4C and D). In all cases, medullary hypoxia followed the medullary DC-shift (by 9.6±1.6 (range 6.5-14) s), while cortical hypoxia preceded the cortical DC-shift (by 18±5.3 (range 9-33) s).

To establish whether respiratory support can re-establish cardiorespiratory and brain activity in *Scn1a*^{L263V} mice stimulated in the inferior colliculus, mechanical ventilation was initiated within

60 s after apnea (n=13). Respiratory resuscitation was successful in 8/13 mice, and more often so if initiated early after apnea onset (Fig. 4D). Recovery of autonomous breathing was always preceded by recovery of brainstem DC-potential (example in SI Appendix, Fig. S2). Sham resuscitation (with the ventilator switched off) initiated <30 s after apnea onset (n=4) was never successful.

FIGURE 4. Sudden apnea in heterozygous *Scn1a*^{L263V} mice is induced by a profound brainstem depolarization.

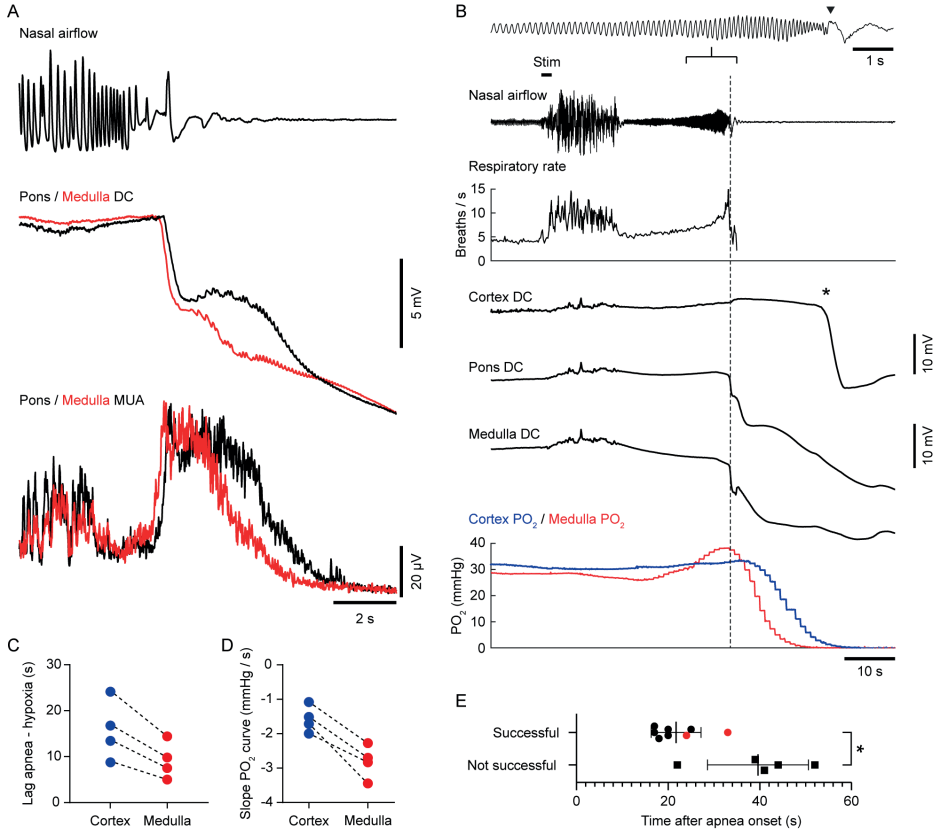

(A) Example of spontaneous and near-simultaneous depolarizations in the pons and medulla of an *Scn1a*^{L263V} mouse. **(B)** Brainstem DC-shifts (onset indicated by dashed line, arrowhead in the inset) following stimulation of the inferior colliculus (Stim) preceded medullary and cortical local PO_2 drops. Note that, on the other hand, the cortical DC-shift followed cortical hypoxia, indicative of an anoxic depolarization (asterisk). **(C)** Following stimulation of the inferior colliculus, medullary hypoxia (PO_2<10 mmHg) consistently preceded cortical hypoxia. **(D)** Local PO_2 consistently decreased faster in the medulla when compared to the cortex. **(E)** Lethality following stimulation of the inferior colliculus could be prevented by timely respiratory resuscitation (*P=0.010; Mann-Whitney test). Resuscitation was also successful during witnessed spontaneous events in two *Scn1a*^{L263V} mice (red).

FIGURE 5. Profound brainstem depolarization in heterozygous *Scn1a*^{L263V} mice preceding spontaneous fatal apnea.

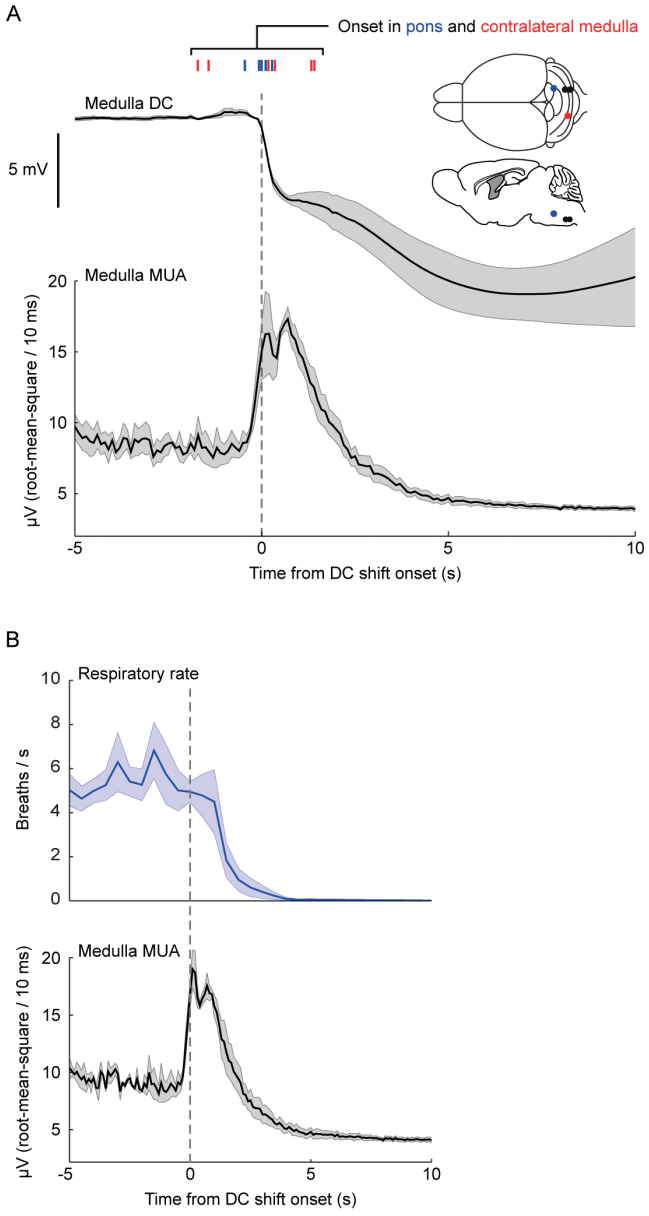

(A) Average DC-signal in the brainstem ventrolateral medulla synchronized at onset of the DC-shift (dashed line at time=0 s). Timing of DC-shift onset in the pons (*n*=5, blue) and contralateral medulla (*n*=6, red) is indicated at the top. Note that an increase in medullary MUA accompanies the negative DC-shift, and is suppressed following the event. **(B)** Average respiratory rate and medullary MUA in *Scn1a*^{L263V} mice (*n*=5) at the time of the medullary DC-shift (dashed line). Note that average MUA is slightly different since only animals with high-quality respiratory recordings are included.

SCN1A^{L263V} causes gain-of-function effects that are reversed by sodium channel blockade

The amelioration of apneic events in our clinical case by CBZ, and the improved breeding of *Scn1a*^{L263V} mice when administered GS967,[18] which promotes use-dependent blockade of sodium channels,[22-24] suggest that sodium channel blockade reduces the abnormalities of the mutant L263V $Na_V1.1$ channels. To test this, we expressed $hNa_V1.1$ in transfected tsA-201 cells and recorded whole-cell sodium currents, comparing the WT and the L263V mutant in the absence or presence of 5 μM GS967 or 15 μM CBZ. The concentration of CBZ used is that found in the cerebrospinal fluid of epileptic patients at standard dosage.[25] There are no data about dosage of GS967 in humans, but previous *in vitro* investigations used it in the micro-molar range.[26, 27] Applying depolarizing steps from a holding potential of -100 mV, we observed robust sodium currents in all groups (Fig. 6A). L263V did not induce a significant modification of maximal current density or voltage-dependence of activation in comparison with WT, whereas both GS967 and CBZ induced a reduction in the former (Fig. 6B). Voltage-dependence of fast inactivation showed a large positive shift induced by the L263V mutation, which was rescued by GS967, but not by CBZ (Fig. 6C). Recovery from fast inactivation was accelerated by L263V (Fig. 6D). GS967 but not CBZ induced a large delay in the recovery that precluded the generation of current in the 20-ms window tested. Current decay, which is induced by inactivation from the open state, was slowed down by L263V (Fig. 6E-G). GS967 completely rescued this effect, whereas CBZ did not. An increase of persistent sodium current (I_{NaP}) for the L263V mutant was not observed (Fig. 6E-G). L263V showed a net decrease of use dependence compared to WT, which was reversed by GS967 but not by CBZ (Fig. 6H-I). Since $Na_v1.1$ is particularly important in fast-spiking GABAergic neurons,[10] we applied as a voltage command its discharge, showing increased action currents in L263V (Fig. 6J-M). GS967 induced a reduction for all the action currents in the discharge, while CBZ induced a smaller reduction in particular during the progression of the discharge.

Overall, the L263V mutant shows a gain of function similar to those previously reported,[9] although we did not observe an increase in I_{NaP}. The limited effect on I_{NaP} is a specific feature of L263V compared to other FHM3 mutants.[14, 27] Sodium channel blockers could revert the effects of the mutation, with GS967 being more effective than CBZ.

FIGURE 6A-6G. Functional modifications induced by L263V on hNa$_v$1.1 and effects of sodium channel blockers GS967 and CBZ.

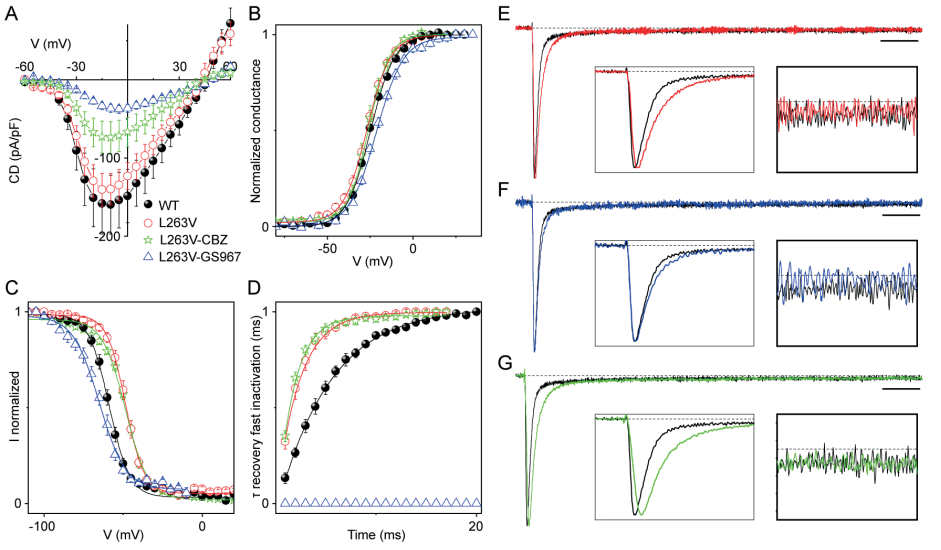

(A) Current density-voltage plots for tsA-201 cells transfected with hNa$_v$1.1-WT (black), hNa$_v$1.1-L263V (red), hNa$_v$1.1-L263V recorded in the presence of 15 μM of CBZ (green) and hNa$_v$1.1-L263V recorded in the presence of 5 μM GS967 (blue). **(B)** Mean voltage-dependence of activation, lines are Boltzmann fits. GS967 induced a 6.1-mV positive shift of the L263V curve (P=0.002), mainly caused by the decrease of the steepness of the curve (20% increase of L263V slope factor, k_d, P=0.007). No statistically significant difference was present between the activation curves of WT, L263V and L263V-CBZ. **(C)** Mean voltage-dependence of fast inactivation, lines are Boltzmann fits. **(D)** Recovery of fast inactivation at -80 mV. (E-G) Comparison of average normalized currents elicited by depolarizing steps to -10 mV for hNav1.1-WT and hNa$_v$1.1-L263V **(E)**, hNa$_v$1.1 and hNa$_v$1.1-L263V-GS967 **(F)**; hNa$_v$1.1 and hNa$_v$1.1-L263V-CBZ **(G)**; calibration bar 5 ms. The left insets show the first 6 ms of the current traces to compare the current decay, the right insets show the traces between 73.5 – 78.5 ms to compare INa_p. (H-I) Use-dependence (current normalized to the first stimulus in the train) induced by trains of 2-ms depolarizing steps to 0 mV from the holding potential of -70 mV at a frequency of 10 Hz

FIGURE 6H-6M. Functional modifications induced by L263V on hNa$_v$1.1 and effects of sodium channel blockers GS967 and CBZ.

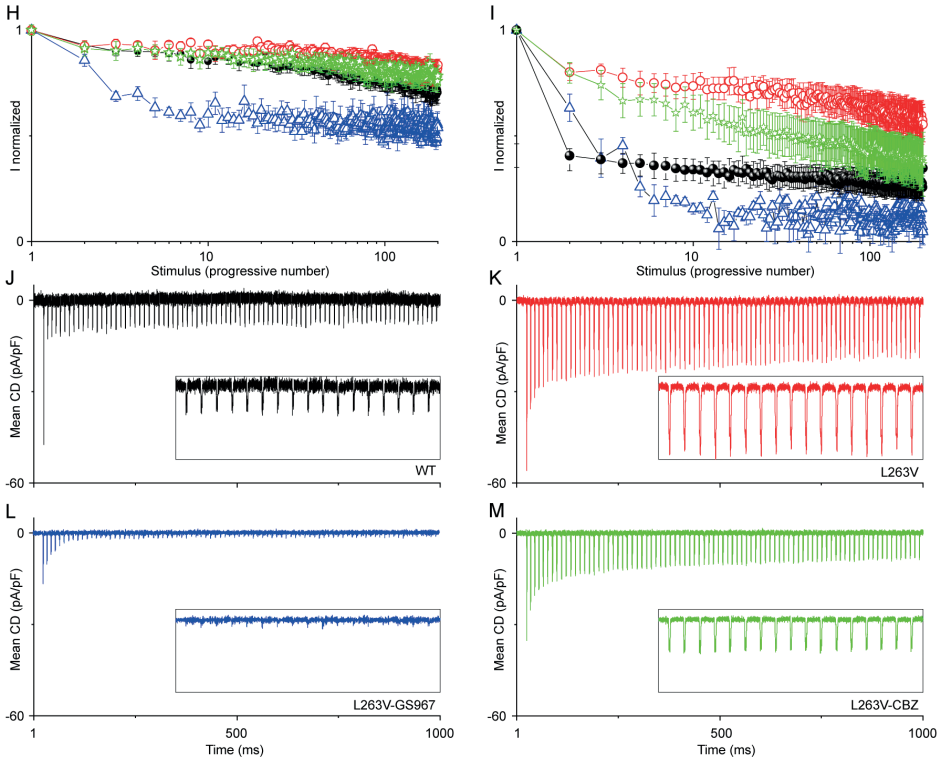

(H) and 100 Hz **(I)** for hNa$_v$1.1-WT, hNa$_v$1.1-L263V, hNa$_v$1.1-L263V-GS967 and hNa$_v$1.1-L263V-CBZ. **(J-M)** Action Na$^+$ currents expressed as mean current density recorded using as voltage stimulus the action potential discharge of a GABAergic fast spiking neuron for hNa$_v$1.1-WT **(J)**, hNa$_v$1.1-L263V **(K)**, hNa$_v$1.1-L263V-GS967 **(L)** and hNa$_v$1.1-L263V-CBZ **(M)**. Data points are displayed as mean ± SEM. See SI Appendix Fig. S3, S4 and Table S1 for statistical comparisons.

Sodium channel blockers prevent brainstem depolarization and apnea in *Scn1a*^{L263V} mice

To test whether sodium channel blockade prevents brainstem DC-shifts, apnea and death *in vivo* in *Scn1a*^{L263V} mice, we evaluated the effects of GS967-compounded chow (8 mg/kg chow). Mice receiving the GS967-compounded chow showed improved survival, while the sudden death phenotype resumed in the days after switching back to normal chow (Fig. 7A). Following stimulation of the inferior colliculus in *Scn1a*^{L263V} mice that received GS967-compounded chow (96±25 μA, compared to 45±7 μA with normal chow; P=0.08, Mann-Whitney test), running behavior was rarely followed by a brainstem DC-shift, apnea or death (Fig. 7B), even when stimulated at more than twice the threshold current. Acute intraperitoneal treatment with GS967

or CBZ prior to stimulation of the inferior colliculus rescued the sudden death phenotype (Fig. 7C). However, pretreatment with MK-801, a potent NMDA receptor antagonist that effectively prevents SD in the preconditioned rat brainstem[20] and in FHM1 mice after stimulation of the inferior colliculus,[19] was ineffective at blocking brainstem DC-shifts, apnea or death in *Scn1a*^{L263V} mice (Fig. 7C). Together, these data indicate that sodium channel blockade impedes lethal apnea in *Scn1a*^{L263V} mice by preventing brainstem DC-shifts.

FIGURE 7. Sodium channel blockers prevent lethal apnea in heterozygous *Scn1a*^{L263V} mice.

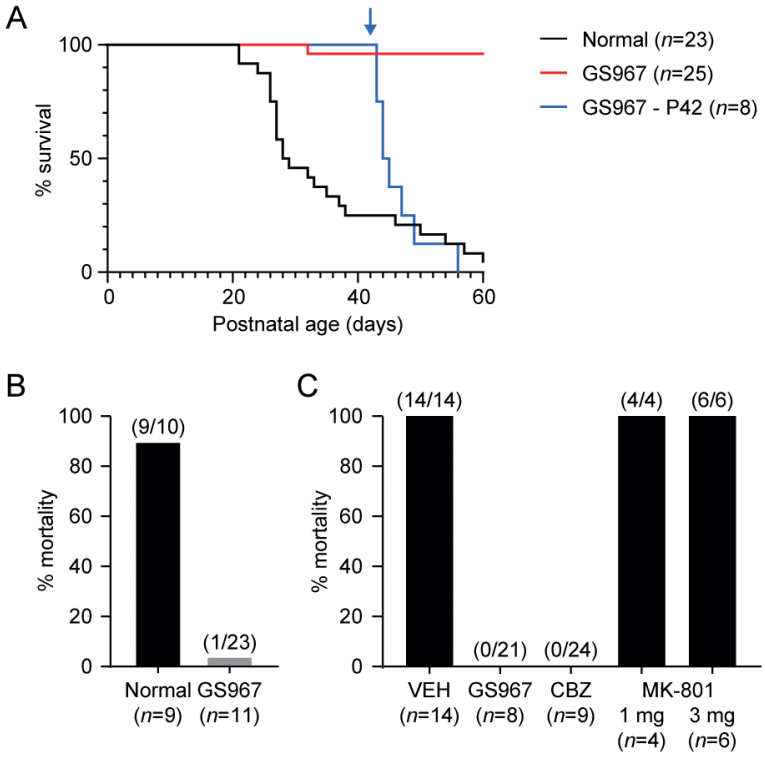

(A) Survival of *Scn1a*^{L263V} mice is improved by chow compounded by GS967 (8 mg/kg chow; red; $P<0.0001$, Mantel-Cox test). In a separate group, withdrawal from GS967 at P42 (blue, arrow) reinstated the sudden death phenotype. **(B)** Stimulation of the inferior colliculus was less likely fatal in mice maintained on GS967-compounded, when compared to normal, chow ($P<0.0001$, Fisher's exact test). **(C)** Intraperitoneal pretreatment with GS967 or CBZ prevented death following stimulation, when compared to vehicle (VEH; $P<0.0001$, Fisher's exact test), whereas MK-801 did not increase survival at the two doses tested ($P>0.99$, Fisher's exact test).

DISCUSSION

We here report a case of an infant with severe and life threatening apneic events, associated with a homozygous *SCN1A*^{L263V} missense mutation. Heterozygous mutation carriers within the family were affected by hemiplegic migraine, consistent with a diagnosis of FHM3, similar to earlier reports.[28, 29] The respiratory phenotype of the clinical case was essentially replicated in *Scn1a*^{L263V} mice, in which a profound brainstem depolarization preceded apnea onset. Sodium channel blockade rescued L263V-associated gain-of-function properties *in vitro*, prevented fatal apnea *in vivo* and decreased the severity of apneic events in the clinical case. These findings indicate that *SCN1A* gain of function can result in life-threatening sudden apnea induced by brainstem dysfunction.

The proband had prolonged periods of apnea that required (cardio)pulmonary resuscitation, suggesting that autoresuscitation following severe hypoxia failed in this child. Failure of autoresuscitation has been implicated in SIDS pathogenesis.[30] Although SIDS is generally believed to occur in sleeping infants, breath-holding during arousal may be an initiating factor in some SIDS cases.[31] We here propose that sudden profound depolarization of brainstem neurons caused by $Na_V1.1$ gain of function can trigger fatal apnea. Previous studies have implicated brainstem SD in epilepsy-related fatal apnea.[19, 32, 33] Here, however, neither the presented clinical case nor *Scn1a*^{L263V} mice showed evidence of seizure activity in behavior or EEG/LFP recordings. Although *Scn1a*^{L263V} mice showed (typically short-lasting) behaviors that may originate from abnormal activity in brainstem centers[34, 35] – behaviors indeed occurred during locally increased MUA and the subsequent DC-shift – convulsive behaviors including clonic or profound tonic activity were never observed. Running behavior was replicated by stimulation of the inferior colliculus in both WT and *Scn1a*^{L263V} mice, and has previously been ascribed to its role in the initiation of aversive states.[36] Interestingly, a recent study described *SCN1A* gain-of-function carriers that presented with seizure-related apnea.[37] Seizure-related brainstem SD was reported in a transgenic FHM1 mouse model[33] and in an *Scn1a* loss-of-function mouse model of Dravet syndrome.[32] In FHM1 mice, SD caused apnea upon propagation to medullary respiratory centers,[19] while SD occurred in the dorsal medulla in Dravet mice.[32] However, NMDA antagonists blocked brainstem SD in previous studies,[19, 20, 32] but did not block brainstem DC-shifts in *Scn1a*^{L263V} mice, suggesting that a different mechanism underlies the profound brainstem depolarization we observed in *Scn1a*^{L263V} mice.

High extracellular potassium renders NMDA antagonists ineffective against SD.[38] Studies have shown that $Na_V1.1$ gain of function leading to hyperexcitability of GABAergic interneurons can facilitate SD initiation because of extracellular potassium build up induced by neuronal spiking,[39, 40] which was confirmed in another FHM3 mouse model in which homozygous *Scn1a*^{L1649Q} knock-in resulted in premature death.[11] A potassium transient may be also caused by $GABA_A$ receptor-mediated redistribution of chloride and bicarbonate and subsequent homeostatic processes.[41, 42] Notably, immaturity of the glial syncytium mediating potassium spatial buffering may increase the susceptibility of the immature brainstem to SD.[43] Indeed, DC-shifts evoked in the

immature rat brainstem are not sensitive to NMDA blockade.[44] Thus, although direct evidence for brainstem DC-shifts in infants may prove difficult to obtain, observations of the clinical phenotype and the presence of DC-shifts in *Scn1a*^{L263V} mice suggest that such profound depolarization should be considered in sudden death pathogenesis.

In addition to insensitivity to NMDA blockade, the delay between brainstem DC-shifts was <2 s in *Scn1a*^{L263V} mice, yielding estimated very high propagation velocities with a median of 1.9 and 7.8 mm/s, between electrodes in medulla-medulla and pons-medulla, respectively. This is in contrast to SD that is characterized by a slower continual spread of a DC-shift at a velocity of a few millimeters per *minute,*[45] suggesting that the present events spread much faster and/or occur at multiple brainstem sites simultaneously. Although hypoxia can cause multifocal SD, which was recently proposed as a mechanism of death in a kainic acid SUDEP mouse model,[46] the PO_2 measurements here indicate that hypoxia is a consequence rather than a cause of the brainstem DC-shift in *Scn1a*^{L263V} mice. In hyperexcitable rat brainstem preparations, DC-shifts propagated at high velocities (up to 30 times faster than SD), roughly similar to observations in *Scn1a*^{L263V} mice, and were also associated with neuronal silencing and prevented by sodium channel blockade.[47] Although the DC-shifts in *Scn1a*^{L263V} mice were invariably fatal and thus showed a persistently negative potential, the initial steep depolarizing phase was of a similar moderate amplitude (a mean of 6.7 mV here, compared to approximately 7-8 mV in previous studies[47]). It was proposed that the high propagation velocities may be facilitated by gap junctions perhaps by allowing fast-propagating Ca^{2+} waves, as earlier reported in the hippocampus.[48, 49] Nevertheless, DC-shifts in *Scn1a*^{L263V} mice show similarities to these fast-spreading events including a characteristic steep negative DC-shift associated with a burst of neuronal activity followed by neuronal silence. Thus, these events may belong to what can be described as the "SD continuum".[50] Estimated propagation velocities in *Scn1a*^{L263V} mice exceeding those earlier published may be explained by focal initiation of the DC-shift in an area between the recording electrodes, or by multifocal initiation that may result from widespread brainstem hyperexcitability due to a high expression of $Na_V1.1$ in brainstem regions.[51, 52]

SCN1A genetic variants have been reported in SIDS cases[5] and sudden unexpected death in pediatrics (SUDP).[4, 53] Seemingly, the gain-of-function effects we report here for *SCN1A*^{L263V} are at odds with loss-of-function effects found with SIDS-associated *SCN1A* mutations.[5] Yet, fatal brainstem SD was first described in a mouse model with a loss-of-function *Scn1a* mutation.[32] Also, *SCN1A* variants associated with SIDS/SUDP are missense and might, instead, show gain of function in a neuronal environment upon rescue of folding/trafficking defects, as it has been reported for some FHM3 mutants.[10, 54] Thus, in addition to *SCN1A*^{L263V}, the risk of brainstem depolarization-induced apnea is likely increased in other *SCN1A* variants. This may explain earlier counterintuitive findings of reduced lethality, despite unchanged or even increased seizure activity, following treatment with sodium channel blockers in epileptic *Scn1a* knockout mice.[55] Similarly, GS967 improved survival in *Scn1a* knockout mice, although this effect could be in part caused

by downregulation of expression of $Na_V1.6$ channels.[22] Brainstem depolarization may thus be a mechanism of sudden death in different *SCN1A* variants.

We report sudden death in both heterozygous and homozygous *Scn1a*^{L263V} mice, whereas severe apneic events were only reported in the homozygous *SCN1A*^{L263V} clinical case. Patients with a heterozygous *SCN1A*^{L263V} mutation in this family, as well as in other families already reported, presented with a phenotype typical of FHM3, not including respiratory dysfunctions, seizures, coma or death related to migraine attacks such as observed in other FHM subtypes.[14] This indicates that the brainstem phenotype of *Scn1a*^{L263V} mice is more severe than in patients, which may be related to interspecies differences in brainstem cytoarchitecture,[56] pattern of $Na_V1.1$ expression, and/or potassium buffering capacity. Alternatively, phenotype severity may be explained by differences in the dimensions of the brainstem and its white matter structures, which effectively interrupt SD propagation.[45] The observational and pharmacological data presented here suggest that brainstem depolarization as observed in our mouse model triggered apneic events in the clinical case. Interspecies differences deserve further attention in future studies to understand the potential risk of profound brainstem depolarizations in other patients.

METHODS

Animals

Scn1a^{L263V} mice were generated by CRIPR/Cas9-mediated homologous recombination as described previously.[18] Mice were maintained on a C57BL/6J background. To improve breeding, heterozygous *Scn1a*^{L263V} male mice used for breeding were maintained on chow containing GS967 (8 mg/kg chow; Research Diets), which was estimated to result in a dosage of 1.5 mg/kg a day.[26] To prevent exposure to GS967 in offspring, male heterozygous *Scn1a*^{L263V} mice received normal chow during the mating period. To generate homozygous *Scn1a*^{L263V} mice, heterozygous male and female *Scn1a*^{L263V} mice continuously received GS967 in food pellets. For behavioral and survival analysis of homozygous *Scn1a*^{L263V} offspring, video recordings from pairs of P14 mice fed with normal chow were obtained, and compared with mice receiving GS967-compounded chow. Approval for experiments was obtained from local and national ethical committees that conformed to the European Communities Council Directive (2010/63/EU). Experiments were carried out in accordance with ARRIVE guidelines.

Surgery

Mice were implanted with platinum/iridium electrodes (75 µm, PT6718, Advent Research Materials) at P19-23 in different configurations: (i) primary visual cortex (-3.5/2.0/0.5; mm relative to bregma, i.e. anterior, lateral and ventral, respectively) and primary motor cortex (+1.5/1.8/0.5), (ii) primary visual and motor cortex, and dorsal (-2.2/2.0/1.3) and ventral (-3.2/3.0/3.5) hippocampus, (iii)

primary visual cortex and brainstem ventrolateral medulla (-6.5/1.3/4.1), and (iv) primary visual cortex, brainstem caudal pontine reticular nucleus (-5.5/1.3/3.9) and ventrolateral medulla. To record MUA, a bipolar electrode was inserted at this location. A reference and ground electrode were placed above the cerebellum. In all mice, a thermistor probe (MEAS-G22K7MCD419, Measurement Specialties) was placed above the nasal epithelium to detect in- and expiration.[57] Two electrodes were inserted in the right and left flank to obtain ECG in a subset of mice. Electrodes were connected to a 7-channel pedestal (MS373; Plastics One), compounded by individual pins (#0489 pin receptacles, Mill-Max), if needed, and secured to the skull using dental cement (DiaDent Europe). Measurements of tissue PO_2 were obtained using a fluorescence-based technique that does not consume oxygen.[58] Probes (230 µm) were inserted in the vicinity of electrodes in the visual cortex (-3.0/2.0/0.5) and ventrolateral medulla (-6.2/1.3/3.8).

In vivo oxygen measurements, pharmacology and resuscitation

For stimulation, a bipolar pulse train (50 Hz, 1-ms pulses) was delivered through a bipolar electrode implanted in the inferior colliculus (-5.0/1.0/0.6) at least 2 days after surgery in WT and heterozygous *Scn1a*^{L263V} mice. Current intensity was increased in steps (20, 50, 100, 200, 500 µA) until running behavior occurred. In case of survival, the current was increased by one step until 3 suprathreshold stimulations were administered. For oxygen measurements, PO_2 was sampled at 1 Hz, starting at least 30 min prior to stimulation.

Respiratory resuscitation (200 breaths/min for 20-120 s, 200 µl/breath) was attempted by positioning a tube connected to a mechanical ventilator (Mini-Vent, Harvard Apparatus) over the nostrils of the animal 17-52 s after apnea onset. As a sham procedure, the ventilator was switched off.

Heterozygous *Scn1a*^{L263V} mice received normal or GS967-compounded chow (8 mg/kg chow) for 2 days prior to stimulation of the inferior colliculus. To test the effect of acute treatment on survival, treatment-naïve mice received an intraperitoneal injection of vehicle, GS967 (1 mg/kg; Cayman Chemical) or CBZ (20 mg/kg; Sigma-Aldrich) 1 h prior to stimulation, or vehicle or MK-801 (1 or 3 mg/kg; Sigma-Aldrich) 30 min prior to stimulation. All injections were performed by an experimenter blinded to the treatment.

Histology

Surviving mice were killed by CO_2 and transcardially perfused. Brains were collected (due to tissue degradation not for all mice that died spontaneously) and postfixed in 4% paraformaldehyde for 2.5 h at 21°C, or for 24 h at 4°C (following spontaneous death), and sucrose-processed. Coronal brain sections (40 µm) were obtained using a sliding microtome (Leica) and Nissl-stained to confirm electrode positions.

Data acquisition and analyses of *in vivo* data

Continuous video-EEG recordings were acquired in a shielded Faraday cage for 2 weeks, or until death of the animal. Both DC- and AC-signals were obtained from brain electrodes, as described previously.[19] MUA was obtained by using the differential signal of bipolar electrodes, and the root-mean-square was calculated over 10-ms bins. Data were analyzed using custom-written MATLAB (MathWorks) scripts. Peak detection was used to calculate instantaneous respiratory and heart rate, and the time of the last peak was used to define onset of apnea and ECG arrest, respectively. EEG suppression was defined as <10% of baseline total EEG power (calculated for 1-100 Hz using a fast Fourier transform).

Plasmids, mutagenesis, cell culture and transfections

For cell transfection, site-directed mutagenesis was achieved by using the shorter splice variant isoform (-11 aa) of the human $Na_V1.1$ a1 channel subunit (GenBank database accession no. NM_006920.4), the predominant $Na_V1.1$ variant expressed in brain also used in earlier studies.[10, 59, 60] The $Na_V1.1$ cDNA was subcloned into the pCDM8 plasmid vector to minimize rearrangements. The L263V mutation was introduced with the Quick Change Lightning Kit (Stratagene), obtaining the mutant $hNa_V1.1$-L263V.

The cell line tsA-201 (Sigma-Aldrich 96121229) was maintained and transiently transfected with $CaPO_4$ as previously reported.[60] Cells were co-transfected with the pCDM8-$hNa_v1.1$ vector and a reporter vector expressing Yellow Fluorescent Protein (pEYFP-N1; Clontech) in order to identify the transfected cells for electrophysiological recordings.

Electrophysiological recordings from transfected cells

Sodium currents were recorded using the whole-cell configuration of the patch-clamp technique as previously reported.[10, 59, 60] Recording solutions (in mM): external solution 150 NaCl, 1 $MgCl_2$, 1.5 $CaCl_2$ and 10 HEPES (pH 7.4 with NaOH); internal pipette solution 105 CsF, 35 NaCl, 10 EGTA, 10 HEPES and (pH 7.4 with CsOH). Voltage dependence of activation was studied applying test pulses of 100-ms from -110 to +60 mV from a holding potential at -120 mV. Voltage dependence of inactivation was studied with a 100-ms prepulse at different potentials followed by a test pulse at -10 mV. Conductance-voltage curves were derived from current-voltage (I-V) curves according to $G=I/(V-V_r)$, where I is peak current, V is test voltage, and V_r is the apparent observed reversal potential for tsA-201. The voltage dependence of activation and the voltage dependence of inactivation were fit to Boltzmann relationships in the form $y=1/(1+\exp((V_{½}-V)/k)$, where y is normalized G_{Na} or I_{Na}, $V_{½}$ is the voltage of half-maximal activation (V_a) or inactivation (V_h) and k is a slope factor; for the inactivation curve we included a baseline. Recovery from fast inactivation was studied using a test pulse at 0 mV followed by a repolarization at -80 mV of different duration and another test pulse. I_{NaP} was quantified as the current during 40-50 ms of the voltage step, expressed as % of maximal transient current (I_{NaT}). Use dependence was evaluated with trains of 200 2-ms-long depolarizing steps to 0 mV from a holding potential of -70 mV at 10 and 100 Hz (leak was subtracted off-line

with a P/3 paradigm). Action potential clamp recordings were performed using as voltage stimulus a discharge recorded from a GABAergic fast-spiking basked cell injecting a 1-s depolarizing current step[39]; the instantaneous firing frequency of the discharge was 82-106 Hz. Recordings were not corrected for junction potentials. GS967 or CBZ were added 15-45 min prior to recordings. Cells were maintained at the holding potential of -100 mV for 5 min prior to recordings.

Statistics

Statistical testing was performed in MATLAB (MathWorks), Graphpad Prism (GraphPad Software) or Origin2021 (Originlab). Data are reported as mean ± SEM, individual data points with mean ± SEM, mean ± standard deviation or box-and-whisker graphs (total range). For *in vivo* data, depending on distribution normality assessed by the Kolmogorov-Smirnov test, the Welch *t*-test or Mann-Whitney test was used for single comparisons. For multiple comparisons, ANOVA or repeated measures ANOVA with Dunnett's test was used. For data obtained in transfected cells, the Kolmogorov-Smirnov test and Levene's test were used prior to comparisons performed with one way ANOVA and Tukey's test. $P < 0.05$ was considered significant.

Acknowledgments

We thank S. van Heiningen for assistance with mouse breeding.

REFERENCES

1. F. J. DiMario, Jr., Breath-holding spells in childhood. *Am J Dis Child* 146, 125-131 (1992).
2. A. Kahn *et al.*, Sleep and cardiorespiratory characteristics of infant victims of sudden death: a prospective case-control study. *Sleep* 15, 287-292 (1992).
3. B. T. Thach, Potential Central Nervous System Involvement in Sudden Unexpected Infant Deaths and the Sudden Infant Death Syndrome. *Compr Physiol* 5, 1061-1068 (2015).
4. H. Y. Koh *et al.*, Genetic Determinants of Sudden Unexpected Death in Pediatrics. *Genet Med* 24, 839-850 (2022).
5. C. A. Brownstein *et al.*, SCN1A variants associated with sudden infant death syndrome. *Epilepsia* 59, e56-e62 (2018).
6. M. Halvorsen *et al.*, Mosaic mutations in early-onset genetic diseases. *Genet Med* 18, 746-749 (2016).
7. R. D. Bagnall *et al.*, Exome-based analysis of cardiac arrhythmia, respiratory control, and epilepsy genes in sudden unexpected death in epilepsy. *Ann Neurol* 79, 522-534 (2016).
8. A. E. Baruteau, D. J. Tester, J. D. Kapplinger, M. J. Ackerman, E. R. Behr, Sudden infant death syndrome and inherited cardiac conditions. *Nat Rev Cardiol* 14, 715-726 (2017).
9. K. M. Kahlig *et al.*, Divergent sodium channel defects in familial hemiplegic migraine. *Proc Natl Acad Sci U S A* 105, 9799-9804 (2008).
10. S. Cestele, E. Schiavon, R. Rusconi, S. Franceschetti, M. Mantegazza, Nonfunctional NaV1.1 familial hemiplegic migraine mutant transformed into gain of function by partial rescue of folding defects. *Proc Natl Acad Sci U S A* 110, 17546-17551 (2013).
11. E. Auffenberg *et al.*, Hyperexcitable interneurons trigger cortical spreading depression in a Scn1a migraine-model. *J Clin Invest* (2021).
12. P. Neligan, D. G. Harriman, J. Pearce, Respiratory arrest in familial hemiplegic migraine: a clinical and neuropathological study. *Br Med J* 2, 732-734 (1977).
13. J. Willson, S. Kapur, Apnoeic spells following general anaesthesia in a patient with familial hemiplegic migraine. *Anaesthesia* 62, 956-958 (2007).
14. M. Mantegazza, S. Cestele, Pathophysiological mechanisms of migraine and epilepsy: Similarities and differences. *Neurosci Lett* 667, 92-102 (2018).
15. M. D. Ferrari, R. R. Klever, G. M. Terwindt, C. Ayata, A. M. van den Maagdenberg, Migraine pathophysiology: lessons from mouse models and human genetics. *Lancet Neurol* 14, 65-80 (2015).
16. J. C. Smith, H. H. Ellenberger, K. Ballanyi, D. W. Richter, J. L. Feldman, Pre-Bötzinger complex: a brainstem region that may generate respiratory rhythm in mammals. *Science* 254, 726-729 (1991).
17. C. A. Del Negro, G. D. Funk, J. L. Feldman, Breathing matters. *Nat Rev Neurosci* 19, 351-367 (2018).
18. N. A. Jansen *et al.*, First FHM3 mouse model shows spontaneous cortical spreading depolarizations. *Ann Clin Transl Neurol* 7, 132-138 (2020).
19. N. A. Jansen *et al.*, Apnea associated with brainstem seizures in Cacna1a (S218L) mice is caused by medullary spreading depolarization. *J Neurosci* 39, 9633-9644 (2019).

20. F. Richter, R. Bauer, A. Lehmenkuhler, H. G. Schaible, Spreading depression in the brainstem of the adult rat: electrophysiological parameters and influences on regional brainstem blood flow. *J Cereb Blood Flow Metab* 28, 984-994 (2008).
21. C. R. Jarvis, T. R. Anderson, R. D. Andrew, Anoxic depolarization mediates acute damage independent of glutamate in neocortical brain slices. *Cereb Cortex* 11, 249-259 (2001).
22. L. L. Anderson, N. A. Hawkins, C. H. Thompson, J. A. Kearney, A. L. George, Jr., Unexpected Efficacy of a Novel Sodium Channel Modulator in Dravet Syndrome. *Sci Rep* 7, 1682 (2017).
23. F. Potet, C. G. Vanoye, A. L. George, Jr., Use-Dependent Block of Human Cardiac Sodium Channels by GS967. *Mol Pharmacol* 90, 52-60 (2016).
24. L. Belardinelli *et al.*, A novel, potent, and selective inhibitor of cardiac late sodium current suppresses experimental arrhythmias. *J Pharmacol Exp Ther* 344, 23-32 (2013).
25. S. I. Johannessen, R. E. Strandjord, Concentration of carbamazepine (Tegretol) in serum and in cerebrospinal fluid in patients with epilepsy. *Epilepsia* 14, 373-379 (1973).
26. L. L. Anderson *et al.*, Antiepileptic activity of preferential inhibitors of persistent sodium current. *Epilepsia* 55, 1274-1283 (2014).
27. R. Barbieri, S. Bertelli, M. Pusch, P. Gavazzo, Late sodium current blocker GS967 inhibits persistent currents induced by familial hemiplegic migraine type 3 mutations of the SCN1A gene. *J Headache Pain* 20, 107 (2019).
28. M. J. Castro *et al.*, First mutation in the voltage-gated Nav1.1 subunit gene SCN1A with co-occurring familial hemiplegic migraine and epilepsy. *Cephalalgia* 29, 308-313 (2009).
29. J. Barros *et al.*, Familial hemiplegic migraine due to L263V SCN1A mutation: discordance for epilepsy between two kindreds from Douro Valley. *Cephalalgia* 34, 1015-1020 (2014).
30. H. C. Kinney, B. T. Thach, The sudden infant death syndrome. *N Engl J Med* 361, 795-805 (2009).
31. B. Thach, Tragic and sudden death. Potential and proven mechanisms causing sudden infant death syndrome. *EMBO Rep* 9, 114-118 (2008).
32. I. Aiba, J. L. Noebels, Spreading depolarization in the brainstem mediates sudden cardiorespiratory arrest in mouse SUDEP models. *Sci Transl Med* 7, 282ra246 (2015).
33. I. C. M. Loonen *et al.*, Brainstem spreading depolarization and cortical dynamics during fatal seizures in Cacna1a S218L mice. *Brain* 142, 412-425 (2019).
34. A. Kreindler, E. Zuckermann, M. Steriade, D. Chimion, Electro-clinical features of convulsions induced by stimulation of brain stem. *J Neurophysiol* 21, 430-436 (1958).
35. T. J. McCown, R. S. Greenwood, G. D. Frye, G. R. Breese, Electrically elicited seizures from the inferior colliculus: a potential site for the genesis of epilepsy? *Exp Neurol* 86, 527-542 (1984).
36. J. E. Pandossio, M. L. Brandao, Defensive reactions are counteracted by midazolam and muscimol and elicited by activation of glutamate receptors in the inferior colliculus of rats. *Psychopharmacology (Berl)* 142, 360-368 (1999).
37. A. Brunklaus *et al.*, The gain of function SCN1A disorder spectrum: novel epilepsy phenotypes and therapeutic implications. *Brain* 145, 3816-3831 (2022).

38. G. C. Petzold *et al.*, Increased extracellular K+ concentration reduces the efficacy of N-methyl-D-aspartate receptor antagonists to block spreading depression-like depolarizations and spreading ischemia. *Stroke* 36, 1270-1277 (2005).
39. O. Chever *et al.*, Initiation of migraine-related cortical spreading depolarization by hyperactivity of GABAergic neurons and NaV1.1 channels. *J Clin Invest* 131 (2021).
40. L. Lemaire *et al.*, Modeling NaV1.1/SCN1A sodium channel mutations in a microcircuit with realistic ion concentration dynamics suggests differential GABAergic mechanisms leading to hyperexcitability in epilepsy and hemiplegic migraine. *PLoS Comput Biol* 17, e1009239 (2021).
41. K. Kaila, K. Lamsa, S. Smirnov, T. Taira, J. Voipio, Long-lasting GABA-mediated depolarization evoked by high-frequency stimulation in pyramidal neurons of rat hippocampal slice is attributable to a network-driven, bicarbonate-dependent K+ transient. *J Neurosci* 17, 7662-7672 (1997).
42. T. Viitanen, E. Ruusuvuori, K. Kaila, J. Voipio, The K+-Cl cotransporter KCC2 promotes GABAergic excitation in the mature rat hippocampus. *J Physiol* 588, 1527-1540 (2010).
43. F. J. Binmoller, C. M. Muller, Postnatal development of dye-coupling among astrocytes in rat visual cortex. *Glia* 6, 127-137 (1992).
44. F. Richter, S. Rupprecht, A. Lehmenkuhler, H. G. Schaible, Spreading depression can be elicited in brain stem of immature but not adult rats. *J Neurophysiol* 90, 2163-2170 (2003).
45. G. G. Somjen, Mechanisms of spreading depression and hypoxic spreading depression-like depolarization. *Physiol Rev* 81, 1065-1096 (2001).
46. A. G. George *et al.*, Sudden unexpected death in epilepsy is prevented by blocking postictal hypoxia. *Neuropharmacology* 231, 109513 (2023).
47. F. Richter, R. Bauer, A. Ebersberger, A. Lehmenkuhler, H. G. Schaible, Enhanced neuronal excitability in adult rat brainstem causes widespread repetitive brainstem depolarizations with cardiovascular consequences. *J Cereb Blood Flow Metab* 32, 1535-1545 (2012).
48. O. Herreras, C. Largo, J. M. Ibarz, G. G. Somjen, R. Martin del Rio, Role of neuronal synchronizing mechanisms in the propagation of spreading depression in the in vivo hippocampus. *J Neurosci* 14, 7087-7098 (1994).
49. P. E. Kunkler, R. P. Kraig, Calcium waves precede electrophysiological changes of spreading depression in hippocampal organ cultures. *J Neurosci* 18, 3416-3425 (1998).
50. J. P. Dreier, C. Reiffurth, The stroke-migraine depolarization continuum. *Neuron* 86, 902-922 (2015).
51. I. Ogiwara *et al.*, Nav1.1 localizes to axons of parvalbumin-positive inhibitory interneurons: a circuit basis for epileptic seizures in mice carrying an Scn1a gene mutation. *J Neurosci* 27, 5903-5914 (2007).
52. T. Furuyama, Y. Morita, S. Inagaki, H. Takagi, Distribution of I, II and III subtypes of voltage-sensitive Na+ channel mRNA in the rat brain. *Brain Res Mol Brain Res* 17, 169-173 (1993).
53. A. M. Rochtus *et al.*, The role of sodium channels in sudden unexpected death in pediatrics. *Mol Genet Genomic Med* 10.1002/mgg3.1309, e1309 (2020).
54. S. Dhifallah *et al.*, Gain of Function for the SCN1A/hNav1.1-L1670W Mutation Responsible for Familial Hemiplegic Migraine. *Front Mol Neurosci* 11, 232 (2018).

55. N. A. Hawkins *et al.*, Screening of conventional anticonvulsants in a genetic mouse model of epilepsy. *Ann Clin Transl Neurol* 4, 326-339 (2017).
56. S. Fujita *et al.*, Cytoarchitecture-Dependent Decrease in Propagation Velocity of Cortical Spreading Depression in the Rat Insular Cortex Revealed by Optical Imaging. *Cereb Cortex* 26, 1580-1589 (2016).
57. S. S. McAfee *et al.*, Minimally invasive highly precise monitoring of respiratory rhythm in the mouse using an epithelial temperature probe. *J Neurosci Methods* 263, 89-94 (2016).
58. J. R. Griffiths, S. P. Robinson, The OxyLite: a fibre-optic oxygen sensor. *Br J Radiol* 72, 627-630 (1999).
59. S. Cestele *et al.*, Divergent effects of the T1174S SCN1A mutation associated with seizures and hemiplegic migraine. *Epilepsia* 54, 927-935 (2013).
60. S. Cestele *et al.*, Self-limited hyperexcitability: functional effect of a familial hemiplegic migraine mutation of the Nav1.1 (SCN1A) Na+ channel. *J.Neurosci.* 28, 7273-7283 (2008).
61. M. Mantegazza *et al.*, Identification of an Nav1.1 sodium channel (SCN1A) loss-of-function mutation associated with familial simple febrile seizures. *Proc Natl Acad Sci U S A* 102, 18177-18182 (2005).

SUPPLEMENTARY MATERIAL

FIGURE S1. Representative examples of hippocampal and cortical activity in a heterozygous *Scn1a*^{L263V} mouse.

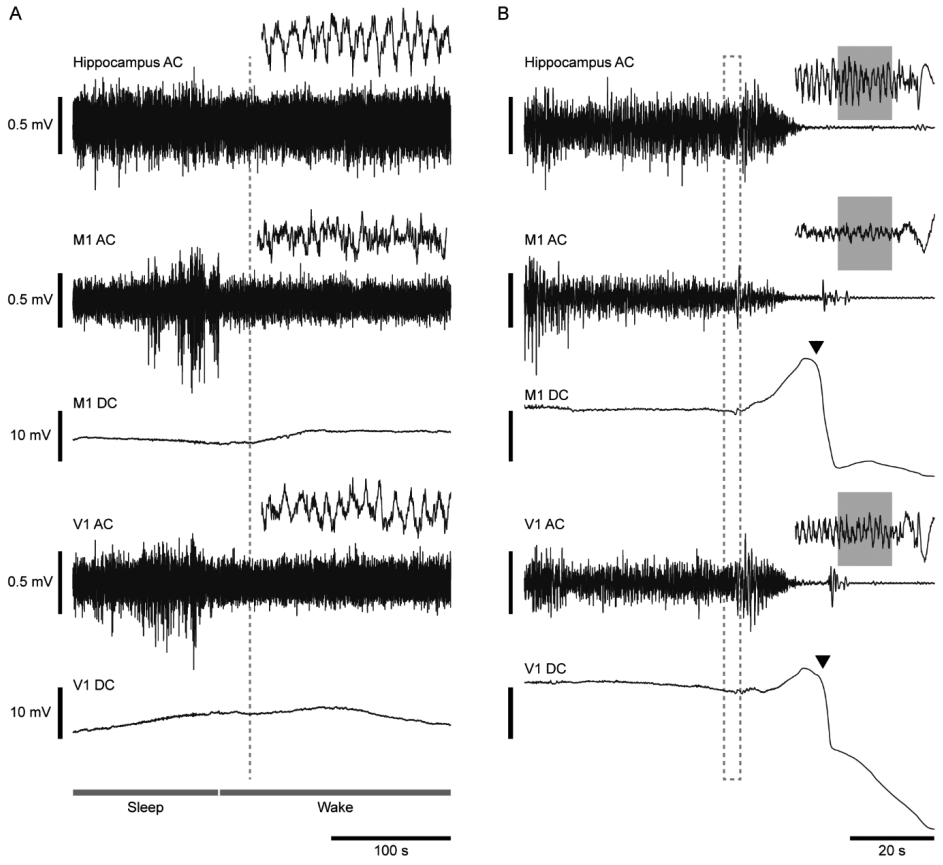

(A) Baseline recordings during sleep and wakefulness. Insets (corresponding with the dashed line, detailing 2 s of local field potential) show characteristic theta wave activity in hippocampus and V1 during movement. Note the moderate-amplitude activity in M1 and V1 during sleep, corresponding with slow waves. No epileptiform activity was noted. **(B)** Recordings during the fatal event showed no epileptiform activity. Insets (corresponding with the dashed box, detailing 4 s of local field potential) show activity during abnormal behavior comprising of change of posture and hindlimb extension (shaded gray).

FIGURE S2. Example of successful respiratory resuscitation of a heterozygous *Scn1a*^{L263V} mouse.

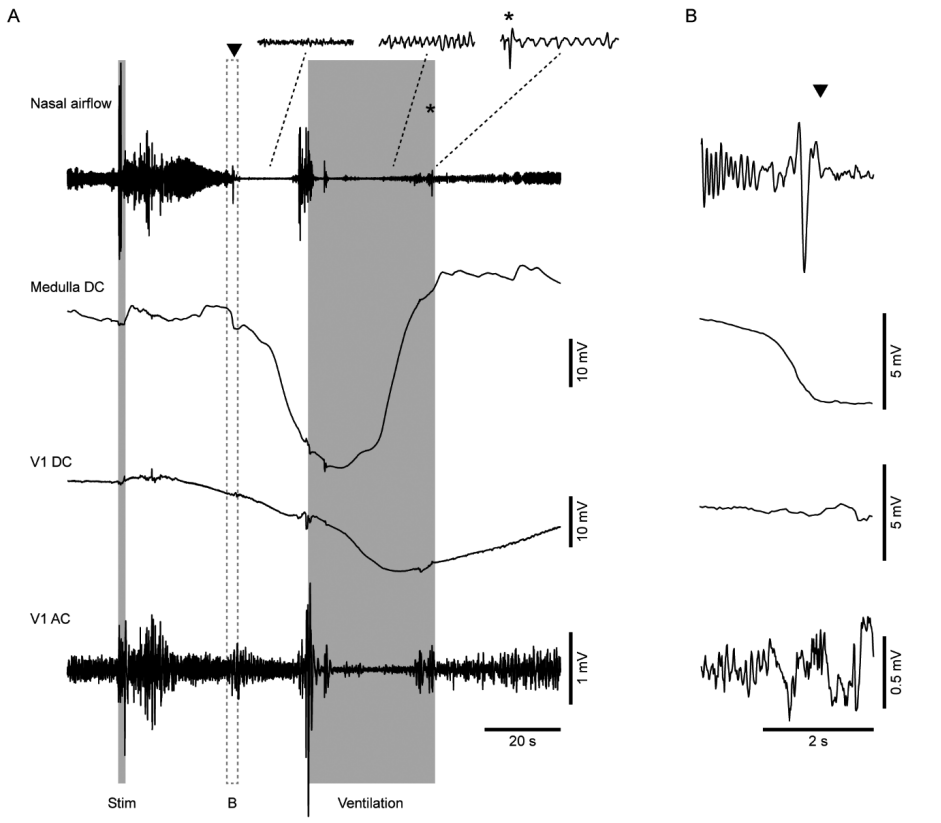

(A) Stimulation of the inferior colliculus (Stim) resulted in a medullary DC-shift followed by apnea (arrowhead; detailed in **B**). During mechanical ventilation (Ventilation), medullary DC-potential recovered prior to the first gasp (asterisk), which was followed by regular breathing. Note that high-amplitude artefacts occurred during stimulation, as well as during positioning the animal immediately prior to mechanical ventilation.

FIGURE S3. Statistical comparisons for functional modifications induced by L263V and effects of 5 µM GS967 and 15 µM CBZ: activation and inactivation properties.

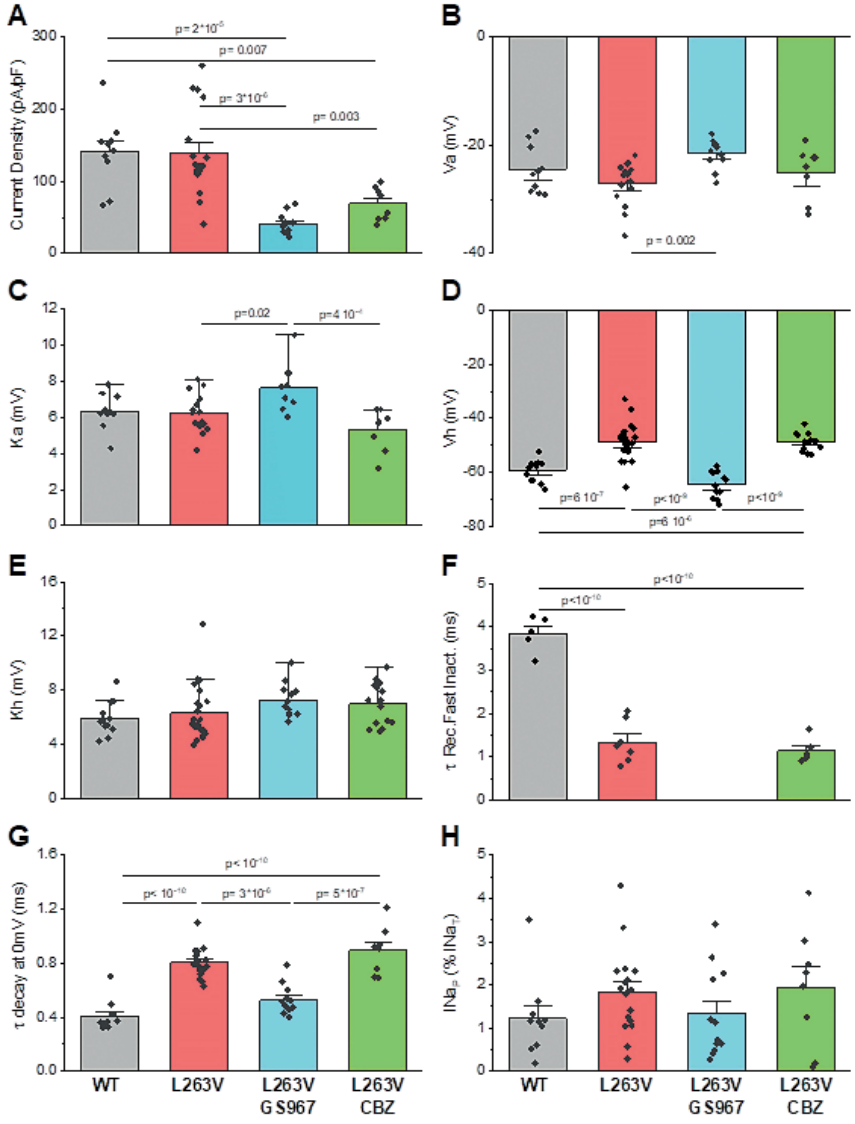

(A) Comparison of maximal current density. **(B)** Comparison of the voltage of half activation (Va) obtained by fits of Boltzmann relationships to the experimental data. **(C)** Comparison of the slope factor of voltage-dependence of activation curves (k_a) obtained by Boltzmann fits of the experimental data. **(D)** Comparison of the voltage of half fast inactivation (Va) obtained by Boltzmann fits of the experimental data. **(E)** Comparison of the slope factor of voltage-dependence of fast inactivation curves (k_h) obtained by Boltzmann fits to the experimental data. **(F)** Comparison of the time constant of recovery from fast inactivation obtained by fits of single exponential relationships to the experimental data. **(G)** Comparison of the time constant of the decay of the current at -10 mV obtained by fits of single exponential relationships to the experimental data. **(H)** Comparison of the maximal INaP. Statistical comparisons have been performed with one way ANOVA followed by Tukey post-hoc test, statistical significant differences ($P < 0.05$) are indicated by solid lines. The bars indicate mean values ± SEM (see also Table S1).

FIGURE S4. Statistical comparisons for functional modifications induced by L263V and effects of 5 μM GS967 and 15 μM CBZ: use dependence and action currents.

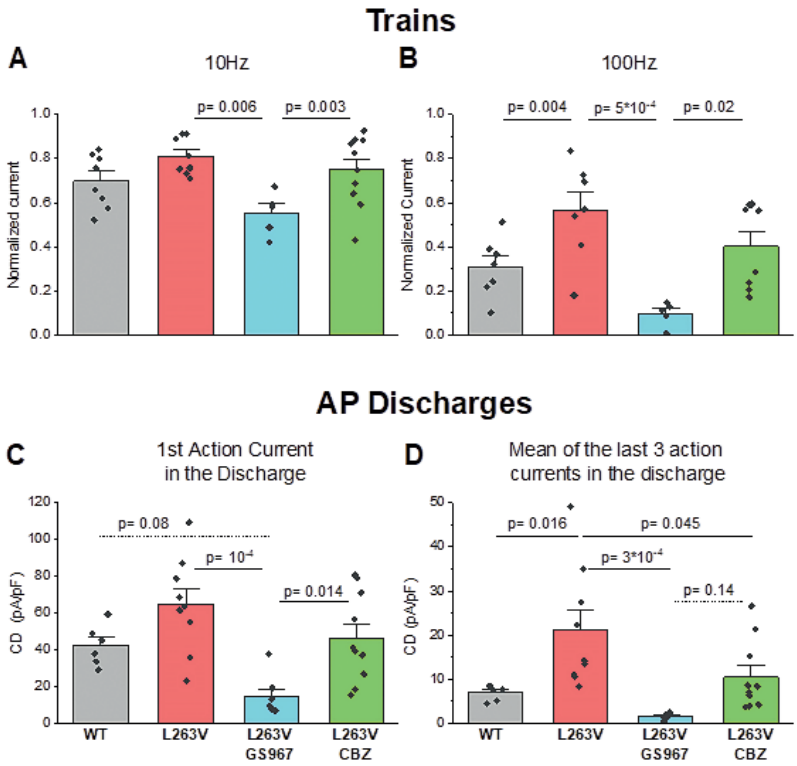

(A) Comparison of use dependence at 10 Hz, evaluating the residual current at the end of a train of 200 2-ms-long depolarizing steps to 0 mV from a holding potential of -70 mV. **(B)** Comparison of use dependence at 100 Hz, evaluating the residual current at the end of a 100-Hz train of depolarizations. **(C)** Comparison of the amplitude of the first action current, expressed as current density, elicited using as voltage command the action potential discharge of a fast spiking GABAergic neuron. **(D)** Comparison of the mean amplitude of the last 3 action currents in the discharge, expressed as current density. Statistical comparisons have been performed with one way ANOVA followed by Tukey post-hoc test, statistical significant differences ($P < 0.05$) are indicated by solid lines, trends by dashed lines. The bars indicate mean values ± SEM (see also Table S1).

FIGURE S5. Medullary electrode locations in heterozygous *Scn1a*^{L263V} mice.

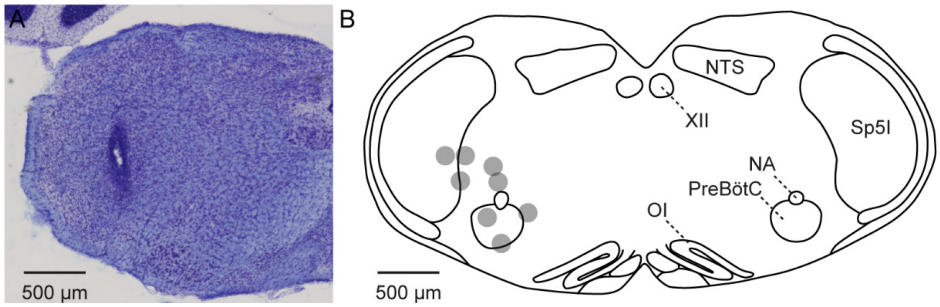

(A) Nissl staining showing an example of an electrode track recovered in an *Scn1a*^{L263V} mouse. **(B)** Schematic of recovered electrode positions (gray dots) in 8 *Scn1a*L263V mice that showed brainstem depolarization and apnea that resulted in death, or that were successfully resuscitated and transcardially perfused. PreBötC, pre-Bötzinger complex; NA, nucleus accumbens; NTS, nucleus tractus solitarius; OI, oliva inferior; Sp5I, spinal trigeminal nucleus pars interpolaris; XII, nucleus hypoglossus.

TABLE S1. Functional properties of sodium currents recorded from tsA-201 cells transfected with hNa$_v$1.1-WT, hNa$_v$1.1-L263V, hNa$_v$1.1-L263V in the presence of 5 µM GS967 and hNa$_v$1.1-L263V in the presence of 15 µM carbamazepine (CBZ). See Figs. S3 and S4 for statistical comparisons.

	WT	L263V	L263V-GS967	L263V-CBZ
Current Density (pA/pF)	140.9 ± 15.2 (*n* = 10)	139.8 ± 14.6 (*n* = 17)	41.0 ± 4.1 (*n* = 12)	69.1 ± 8.2 (*n* = 8)
Va (mV)	-24.5 ± 1.4 (*n* = 10)	-27.1 ± 1.0 (*n* = 17)	-21.4 ± 2.7 (*n* = 12)	-25.0 ± 1.7 (*n* = 8)
Ka (mV)	6.4 ± 0.3	6.3 ± 0.3	7.6 ± 0.4	5.3 ± 0.4
Vh (mV)	-59.2 ± 1.1 (*n* = 13)	-48.6 ± 1.3 (*n* = 24)	64.4 ± 1.4 (*n* = 12)	48.8 ± 0.8 (*n* = 15)
Kh (mV)	5.9 ± 0.3	6.3 ± 0.4	7.3 ± 0.4	7.0 ± 0.4
τ Recovery from Fast Inactivation at -80mV (ms)	3.8 ± 0.2 (*n* = 5)	1.3 ± 0.2 (*n* = 7)	- (*n* = 6)	1.1 ± 0.1 (*n* = 6)
τ Current Decay at 0mV (ms)	0.41 ± 0.04 (*n* = 10)	0.80 ± 0.03 (*n* = 17)	0.53 ± 0.03 (*n* = 12)	0.89 ± 0.06 (*n* = 8)
INa_{PMax} (% INa_{TMax})	1.2 ± 0.3 (*n* = 10)	1.8 ± 0.2 (*n* = 17)	1.3 ± 0.3 (*n* = 12)	1.9 ± 0.5 (*n* = 8)
Use dependence at 10 Hz (fraction of the initial current)	0.70 ± 0.04 (*n* = 8)	0.81 ± 0.03 (*n* = 8)	0.55 ± 0.04 (*n* = 5)	0.75 ± 0.05 (*n* = 10)
Use dependence at 100 Hz (fraction of the initial current)	0.31 ± 0.05 (*n* = 7)	0.56 ± 0.08 (*n* = 7)	0.09 ± 0.02 (*n* = 5)	0.40 ± 0.07 (*n* = 8)
1st action current in the FS discharge (pA/pF)	42.2 ± 4.5 (*n* = 6)	64.7 ± 8.6 (*n* = 9)	14.9 ± 3.7 (*n* = 8)	46.5 ± 7.7 (*n* = 10)
Average of last 3 action currents in the FS discharge (pA/pF)	6.9 ± 0.7 (*n* = 6)	21.3 ± 4.6 (*n* = 9)	1.6 ± 0.2 (*n* = 8)	10.5 ± 2.5 (*n* = 10)

Movie S1 (separate file). Example of cortical activity during a fatal event in an *Scn1a*^{L263V} mouse. The animal shows a sudden change of posture and subtle hindlimb extension, in total lasting approximately 1-2 s, followed by suppression of cortical activity and finally cortical anoxic depolarization. Note the absence of cortical epileptiform activity.

Movie S2 (separate file). Example of behavior during the fatal event in an *Scn1a*^{L263V} mouse. The animal shows exploratory behavior followed by drinking, during which a sudden change of posture occurs with loss of balance and subtle hindlimb extension.

Movie S3 (separate file). Example of brainstem DC-shift during the fatal event in an *Scn1a*^{L263V} mouse. The animal shows a sudden change of posture that co-occurs with a DC-shift in the medulla, which is repeated in slow-motion at the end.